Received: 23 September 2022 | Revised: 30 November 2022 | Accepted: 4 January 2023

DOI: 10.1111/ijag.16623

INTERNATIONAL JOURNAL OF Applied Glass SCIENCE

RESEARCH ARTICLE

Effect of draw temperature and flame polishing on birefringence of silica glass fiber

Bronson D. Hausmann[1] | **Thomas W. Hawkins**[2] | **John Ballato**[2] | **Minoru Tomozawa**[1]

[1]Department of Materials Science and Engineering, Rensselaer Polytechnic Institute, Troy, New York, USA

[2]Center for Optical Materials Science and Engineering Technologies (COMSET) and the Department of Materials Science and Engineering, Clemson University, Clemson, South Carolina, USA

Correspondence
Minoru Tomozawa, Department of Materials Science and Engineering, Rensselaer Polytechnic Institute, Troy, 12180 NY, USA.
Email: tomozm@rpi.edu

Funding information
NSF, Grant/Award Number: DMR-1713670

Abstract

Recently developed methods for high resolution birefringence measurement have been applied to distinguish between the surface and interior birefringence of silica glass fibers as a function of drawing temperature and initial surface condition for two types of silica glass with different water contents. Fibers were drawn in a water-free argon environment using graphite heating elements. It was found that fibers drawn at lower temperatures resulted in greater, interior birefringence, in agreement with previous reports. Additionally, it was found that in the case of low-water silica glass, flame polishing via oxygen–hydrogen mixture and drawn into fibers at lower temperature resulted in significant surface compressive stress upon drawing. This compressive stress may be the result of surface stress relaxation in silica glass that occurs in the presence of water during fiber drawing. In silica glass that contains greater internal hydroxyl impurity concentrations, the interior birefringence as well as the surface stress relaxation was significantly reduced under the same fiber drawing conditions. Characterization of such stress responses provides insight into the effects of common processing techniques as well as impresses the significance of preform processing for consistent fiber production.

KEYWORDS

birefringence, characterization, glass products, optical fibers, optical properties, silicate, surfaces

1 | INTRODUCTION

Glass structure is highly dependent on processing temperature, cooling rate, and atmospheric water content.[1–6] Drawn glass fibers, in particular, undergo very dramatic temperature changes over short time scales, resulting in a high degree of such sensitivity.[7–10] Fibers have been previously characterized using birefringence measurements as a function of draw temperature and draw rate, with results indicating that lower temperatures and higher draw rates have a similar effect of increasing birefringence.[7,11,12] Fibers produced for this work were 125 μm in diameter, the same diameter as the commercial optical fibers but had no core with different compositions. Therefore, stresses due to temperature gradient[13] and different compositions of core/cladding[14–16] are absent. Birefringence in glass is related to residual stress or a result of structural anisotropy. The residual stress is linear with applied strain, and

TABLE 1 Fiber samples employed in this work along with selected properties and process conditions

Sample	Material	Manufacture process	Draw temperature (°C)	Flame polished	T_g (°C)	OH (wt. ppm)	Cl (wt. ppm)
A	F300	Flame hydrolysis	1875	Yes	1150	<.1	800–2000
B				No			
C			1950	Yes			
D				No			
E	T08	Fusion	1875	Yes	1155	180	~0
F			1950	Yes			

Note: Data from preform manufacturer were available. In the case of T08, the glass transition temperature and water content have been measured, and no Cl has been detected.[4]

birefringence is often discussed in terms of stress, σ (in MPa), via the stress-optic relation:

$$\sigma = \frac{\Delta}{C \cdot y} \tag{1}$$

where Δ is the retardance (in nm), C is the stress-optic coefficient (in Brewsters, MPa^{-1}), and y is the path length of the material being measured (in mm). Retardance is measured using polarized light microscopy via various methods. In this work, as detailed later, the Sènarmont method is employed as it represents a common method for measuring small values of retardance.[17–21]

2 | PROCEDURE

2.1 | Materials and fiber drawing

Two silica glass preforms were selected for this work: Heraeus F300 and Heraeus T08. The most significant difference between the selected silica glass preforms is the OH impurity content. F300 silica is produced through a vapor deposition process resulting in less than .1 wt. ppm of OH impurity, whereas T08, a silica glass made from the fusion of natural quartz, is known to contain 180 wt. ppm OH.[4] Despite the vast difference in OH impurity, the glass transition temperatures for the two silica glasses are nearly equivalent due to the high Cl impurity within F300 reducing the glass transition temperature, T_g, to a similar degree (Table 1).

Flame polishing of some silica glass preforms was carried out using an oxygen–hydrogen torch. An even application was assured using an SG Controls modified chemical vapor deposition lathe, equivalent to those conventionally used for optical fiber preform fabrication (Clemson University, Clemson, SC, USA). The lathe applied the flame evenly via rotation of the silica glass rod during polishing. This is a common technique to mitigate surface irregularities upon the preform but has also been known to introduce significant OH content into the preform surface.[22]

Optical fibers were drawn using a Heathway draw tower (Clemson University, Clemson, SC, USA) from the two types of silica glass rods (Heraeus F300 and Heraeus T08) to the same diameter of 125 μm (conventional diameter used for commercial optical fibers) to compare the effects of water impurity concentration and drawing parameters on as-drawn fiber retardance (Table 1). Fiber drawing was performed in an argon environment using a graphite resistance heating element. Two draw temperatures were chosen and employed for both types of glass rods: 1875 and 1950°C. Thus, a greater draw tension was applied during the lower temperature draw to achieve the same target diameter of 125 μm while maintaining a constant draw rate. Following drawing, the fibers were coated in a conventional optical fiber polymer coating (Desotech DSM 3471-3-14), which was subsequently removed before retardance measurement by soaking in acetone for 60 s to induce swelling, followed by mechanical stripping. This method avoids unnecessary further heating of the fiber.

2.2 | Retardance profiles

To characterize the compressive stress observed in the low-temperature, flame-polished F300 fiber (sample A), the retardance profile was fit to a model of surface stress relaxation, based on the complimentary error function (Figure 1)[20]:

$$\sigma_{res}(x,z) = \sigma_{applied}\left\{\operatorname{erf}\left(\frac{r_o - x}{2z}\right) - \frac{2}{r_o^2}\int_0^{r_o} \operatorname{erf}\left(\frac{r_o - x}{2z}\right)\cdot x\, dx\right\} + k, \tag{2}$$

where $\sigma_{res}(x,z)$ is the residual stress at position x along the fiber cross section with a characteristic surface layer

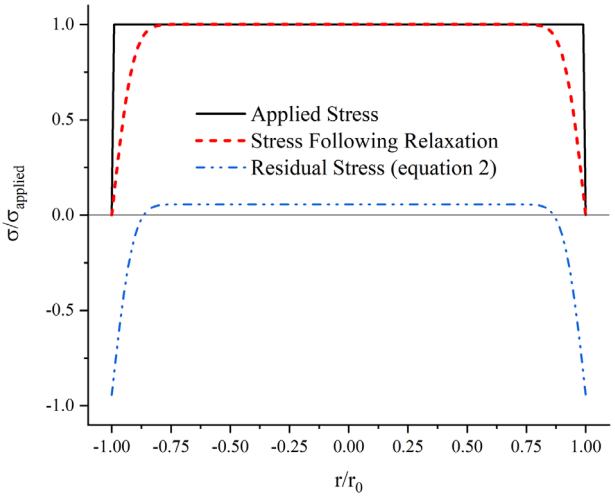

FIGURE 1 Example of the curve produced by Equation (2) where x ranges from zero to a theoretical radius of r_o and with a relaxation depth of $z = .05r_o$. The offset constant k is zero but can visualize as a vertical shift of the entire curve.

relaxation depth of z, at which point the error function magnitude reaches 50%. $\sigma_{applied}$ is the assumed-constant applied stress during relaxation, r_0 is the fiber radius, and k is the remaining, interior birefringence which is not accounted for by a balance of elastic forces, usually positive.[20]

Fiber retardance profiles were measured using the Sènarmont method, in which the retardance is calculated from the degree of rotation of polarized light passing through the diameter fiber (Figure 2). Measurements obtained by this method allow for calculation of retardance, Δ, through the following relation:

$$\Delta = \lambda \cdot \frac{\delta(\theta_{min})}{360} \quad (3)$$

where λ is the wavelength of light used during measurement (546 nm in this work), δ is the relative retardation in degrees, and 360 is the conversion factor from degrees to wavelength necessary for retardance. Comparisons of the measured profiles were made by the measurement of the average interior birefringence k. This was necessary in the case of fibers demonstrating only birefringence as a result of tensile deformation. The force balance that was assumed in the development of Equation (2) for use in an analysis of relaxation and elastic response of surface stress relaxation does not describe the retardance found in such fibers.

3 | RESULTS

Fibers containing higher impurity OH (sample E and F) were found to demonstrate significantly lower, interior, retardance, whereas fibers drawn at the lower temperature of 1875°C demonstrated greater retardance compared to the fibers which were drawn at the higher temperature (Figure 3). Sample A demonstrated a negative retardance near the fiber surface, corresponding to a compressive strain. This sharp surface compressive stress was observed only in sample A (Figure 4).

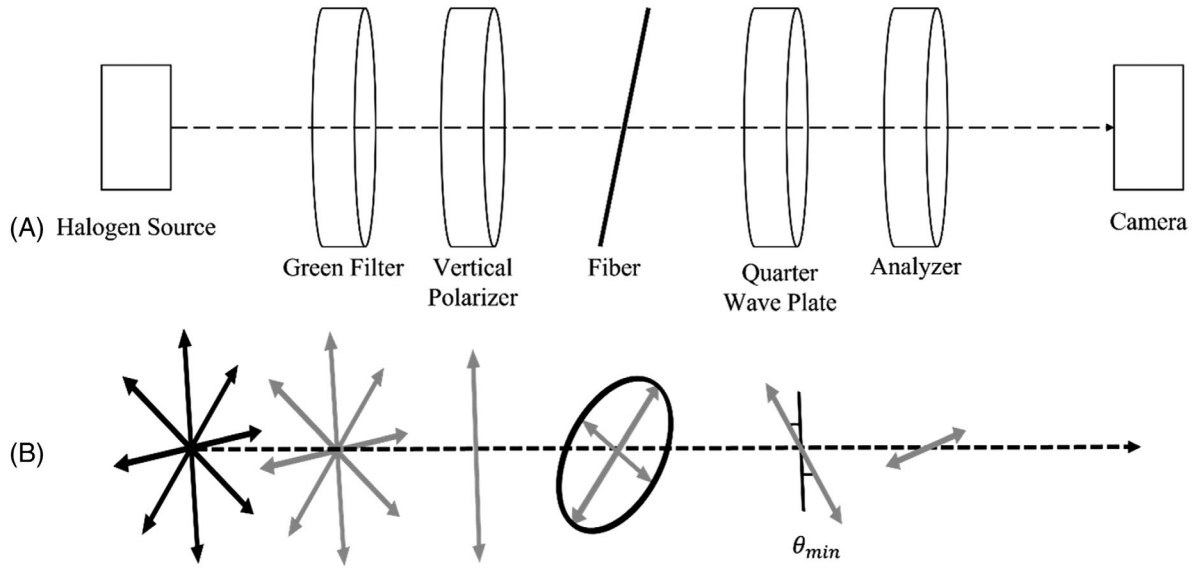

FIGURE 2 (A) Schematic of the microscope configuration used for the Sènarmont method. The sample is placed at a 45° angle between crossed polarizers along with a quarter wave plate which is paired with a light filter of appropriate wavelength (546 nm via interference filter). (B) Polarization state of light as it passes through the microscope. The light is elliptically polarized as it passes through the sample. Elliptically polarized light is then converted to linearly polarized light of a new rotation angle θ_{min}, which is inferred via rotation of the analyzer.

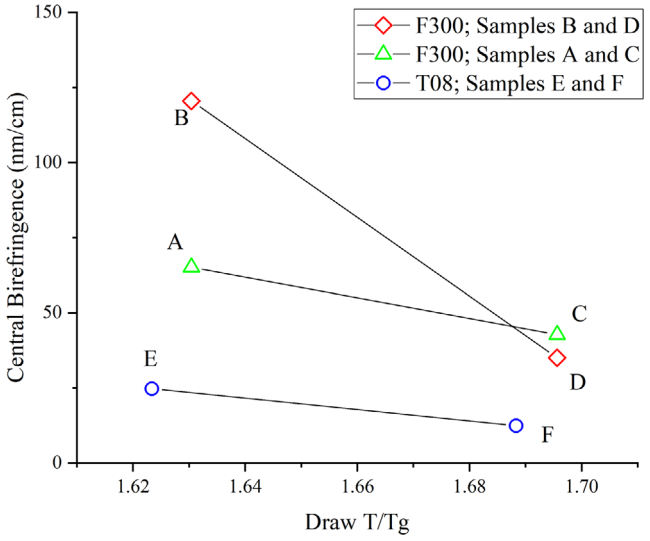

FIGURE 3 Average interior or "central" birefringence of fibers as a function of draw temperature, normalized by T_g. Values are obtained by calculating the average birefringence of the measured retardance profiles. Error in y direction is smaller than the size of the data point (±1 nm/cm).

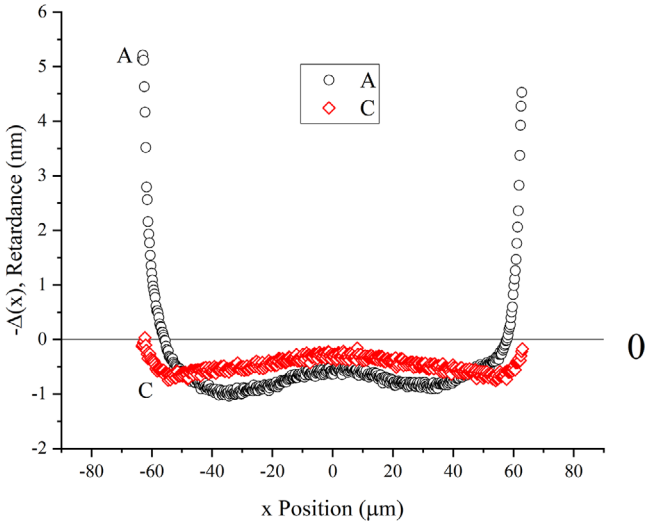

FIGURE 4 Retardance profile of F300 fibers, samples A and C, which were flame-polished with an oxy–hydrogen torch before drawing. A surface compressive stress is evident in sample A, which was drawn at 1875°C.

Parameters of analogous applied stress, relaxation depth, and bulk nonelastic birefringence were found by least squares fitting of Equation (2) and are listed in Table 2. In order to convert the stress relaxation model parameters into a fit of retardance, an additional integration is required to account for the circular cross section of the fiber, which results in a path length, y in Equation (1), that varies with measurement position, x:

TABLE 2 Fit parameters for Equation (4), as shown in Figure 5

$\sigma_{applied}$ (GPa)	.7632 ± .2
k (nm/mm)	1.571 ± .06
z (μm)	.223 ± .05

Note: Intervals are 95% confidence intervals for the fitted parameters.

$$\Delta(x) = \int_{y_{\min}=-\sqrt{r_0^2-x^2}}^{y_{\max}=\sqrt{r_0^2-x^2}} C \cdot \sigma_{res}(x,z)\, dy \qquad (4)$$

Plots of retardance shown here place negative retardance values on the positive y axis (corresponding to compressive stress) in order to match the convention used in the characterization of tempering and ion exchange stress profiles, where compressive stress is expected (Figure 5).

The model assumes that water interaction is necessary for relaxation to occur. As the fiber is drawn in a water-free environment, only internal water present due to the flame polishing may contribute. F300 fibers produced without flame polishing did not exhibit surface compression (Figures 4 and 6) but instead demonstrated a greater degree of tensile deformation. T08 fibers exhibited markedly lower retardance overall, with the 1875°C drawn fiber having slightly greater retardance than the 1950°C fiber (Figure 6). Many fibers only demonstrated retardance corresponding to tensile stress. Equation (2) was unable to describe such measured profiles. Instead, a fit of a single birefringence value was chosen to compare between fibers. Birefringence is proportional to retardance per unit path length of material. It is thus possible to estimate a

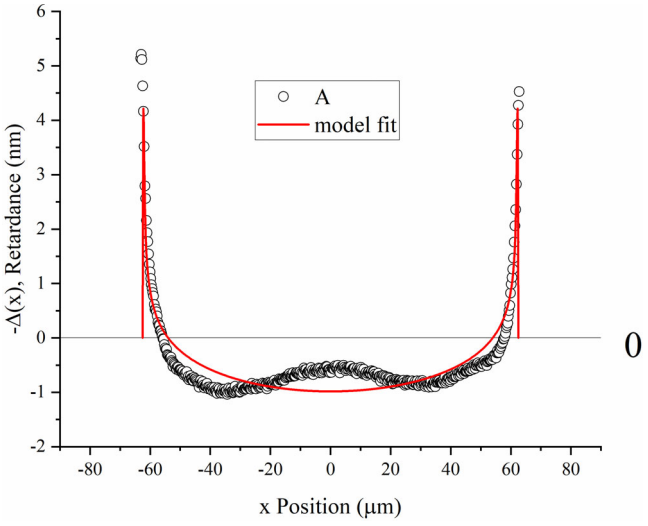

FIGURE 5 Fit of Equation (4) to sample A, fit to the proposed model for surface stress relaxation in the presence of water

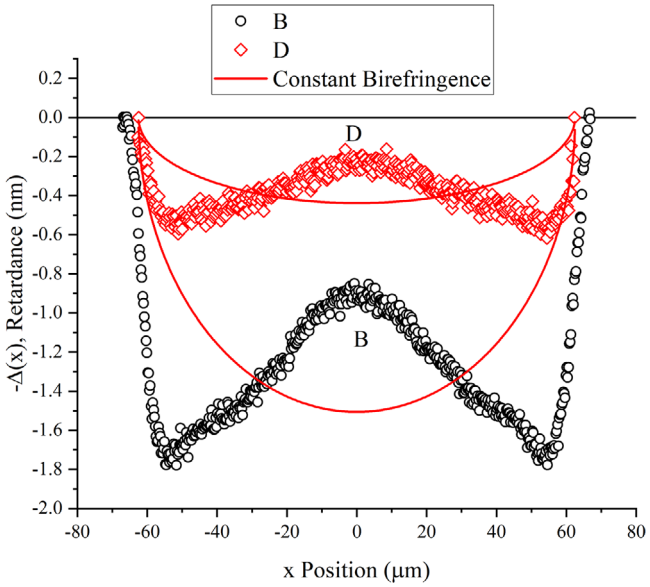

FIGURE 6 Retardance profile of F300 fiber, samples B and D, which were not flame-polished before drawing. Also included are curves of constant birefringence illustrating the deviation observed in the F300 fibers.

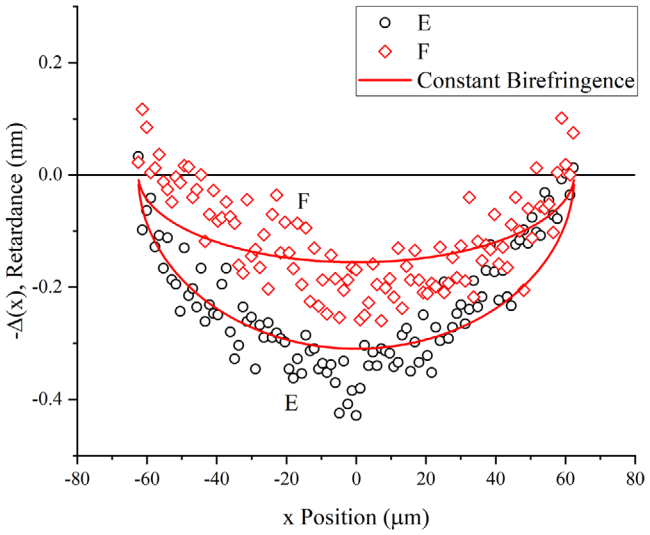

FIGURE 7 Retardance profile of T08 fiber, samples E and F, including a fit of constant birefringence

best fit for samples where only tensile stress was observed. This is indicated in Figures 6 and 7 as lines of constant birefringence.

4 | DISCUSSION

Significant decrease in retardance with increasing fiber draw temperature (Figure 3) is likely a result of the decreased viscosity allowing for more rapid relaxation of the fiber. The 50° increase in draw temperature chosen for this work corresponds to roughly a factor of 5 decrease in viscosity for silica.[2,23,24] Temperature dependance in as-drawn fiber retardance has been observed previously and has been attributed to the anisotropy of network motifs aligning during the drawing process.[8,9]

4.1 | Different fiber interior anisotropies form in the fibers of F300 (Figures 4–6) versus T08 (Figure 7)

Fibers of F300 exhibited wavy anisotropy profiles interior of the fiber, whereas T08 exhibited smooth circular anisotropy profiles with the value of k nearly constant. The difference can be attributed to the difference of manufacturing processes of the silica glasses. The form of the anisotropy profile of the F300 fiber indicates the diminishing value of the anisotropy at the fiber center. It is known that silica glass preform for waveguides has frequently been produced using the outside vapor deposition (OVD) technique, having in a hollow in the center.[25] The preforms chosen for this work were presumably collapsed into solid rods from existing OVD preform with a hollow center. This may account for a silica glass rod with a slightly different structure in the center of the F300 preform due to fictive temperature differences, which can lead to the difference in curvature observed in the center of such F300 samples.

4.2 | Effect of flame polish on surface compressive stress of fibers prepared at different temperatures

Only fibers made of F300 at lower temperature after flame polishing exhibited surface compressive stress, which is due to surface stress relaxation, whereas other silica glass fibers did not.

Flame polishing with oxy–hydrogen can result in increased water (OH) content at the fiber preform surface.[22] Ref. [22] demonstrates a diffusion depth of 50–100 μm at a concentration of 600–900 wt. ppm. Such a degree of OH impurity is in the same order as is found throughout T08 and likely influences the surface of the F300 fiber to relax accordingly. Because the fiber drawing is a relatively fast process, however, it is not limited by this depth but instead by the relaxation rate (resulting in the low value of z found for Equation 2). This is likely to enable surface stress relaxation during fiber drawing of the flame-polished F300 fiber, and thus producing the observed compressive stress.[26,27] However, when silica glass with high Cl content is heat-treated, Cl can evaporate

and its surface viscosity increases and cause the slower surface structural relaxation.[28] Similarly, water evaporation from silica glass via dehydration reaction can take place when water-containing silica glass was heated causing the glass viscosity to increase. This evaporation may be the reason why surface stress relaxation was not observed for most silica glass fibers containing a high concentration of OH or chlorine in the preform.

This is further confirmed by the ability to fit the flame-polished sample stress profile with some success to the surface stress relaxation model. The fact that the higher bulk water content glass, T08, exhibits significantly lower surface compressive stress even having applied the same flame polishing procedure suggests that in the case of a uniformly high OH impurity glass, relaxation may occur throughout the material more readily due to the decreased viscosity caused by the OH impurity. Despite the decreased magnitude of birefringence in T08, the fact that a compressive stress is still observed in T08 at the lower temperature in addition to the significant decrease in overall birefringence suggests that flame polishing does impart greater surface water impurity than initially present in the glass overall.

5 | CONCLUSION

It has been demonstrated that fiber draw temperature and fiber preform processing can greatly influence the strain present in a drawn silica fiber. In the case of preforms treated via oxy–hydrogen flame polishing, significant surface stress relaxation can occur especially at lower draw temperatures. This is likely due to surface stress relaxation caused by water present in the preform surface. The features observed in the F300 fiber indicate that interior tensile deformation is likely a result of the fiber preform production process.

ACKNOWLEDGMENT

This research was supported at Rensselaer by the NSF grant DMR-1713670 and Corning Inc, and at Clemson by the J. E. Sirrine Foundation.

ORCID

Bronson D. Hausmann https://orcid.org/0000-0003-1448-3392

John Ballato https://orcid.org/0000-0001-5910-3504

REFERENCES

1. Brückner R. Properties and structure of vitreous silica. I. J Non-Cryst Solids. 1970;5(2):123–75. https://doi.org/10.1016/0022-3093(70)90190-0
2. Brückner R. Properties and structure of vitreous silica. II. J Non-Cryst Solids. 1971;5(3):177–216. https://doi.org/10.1016/0022-3093(71)90032-9
3. Koike A, Ryu SR, Tomozawa M. Adequacy test of the fictive temperatures of silica glasses determined by IR spectroscopy. J Non-Cryst Solids. 2005;351(52):3797–803. https://doi.org/10.1016/j.jnoncrysol.2005.10.005
4. Agarwal A, Davis KM, Tomozawa M. A simple IR spectroscopic method for determining fictive temperature of silica glasses. J Non-Cryst Solids. 1995;185(1):191–8. https://doi.org/10.1016/0022-3093(94)00676-8
5. Davis KM, Tomozawa M. Water diffusion into silica glass: structural changes in silica glass and their effect on water solubility and diffusivity. J Non-Cryst Solids. 1995;185(3):203–20. https://doi.org/10.1016/0022-3093(95)00015-1
6. Ya M, Deubener J, Yue Y. Enthalpy and anisotropy relaxation of glass fibers. J Am Ceram Soc. 2008;91(3):745–52. https://doi.org/10.1111/j.1551-2916.2007.02100.x
7. Murach J, Brückner R. Preparation and structure-sensitive investigations on silica glass fibers. J Non-Cryst Solids. 1997;211(3):250–61. https://doi.org/10.1016/S0022-3093(96)00635-7
8. Stockhorst H, Brückner R. Structure sensitive measurements on e-glass fibers. J Non-Cryst Solids. 1982;49(1):471–84. https://doi.org/10.1016/0022-3093(82)90140-5
9. Murach J, Jander S, Brückner R. Structure-sensitive investigations on alkali disilicate glass fibers with reference to metasilicate- and silica glass fibers. J Non-Cryst Solids. 1997;217(1):92–8. https://doi.org/10.1016/S0022-3093(97)00156-7
10. Chu PL, Whitbread T. Measurement of stresses in optical fiber and preform. Appl Opt. 1982;21(23):4241. https://doi.org/10.1364/AO.21.004241
11. Brückner R, Habeck A. Anisotropic optical properties and flow behaviour of mechanically deformed single-phase glass melts. Glastech Ber Glass Sci Technol. 1994;67(1):1–8.
12. Habeck A, Brückner R. Direct connection between anisotropic optical properties, polarizability and rheological behaviour of single-phase glass melts. J Non-Cryst Solids. 1993;162(3):225–36. https://doi.org/10.1016/0022-3093(93)91241-T
13. Paek UC, Kurkjian CR. Calculation of cooling rate and induced stresses in drawing of optical fibers. J Am Ceram Soc. 1975;58(7–8):330–5. https://doi.org/10.1111/j.1151-2916.1975.tb11490.x
14. Yablon AD, Yan MF, DiGiovanni DJ, Lines ME, Jones SL, Ridgway DN, et al. Frozen-in viscoelasticity for novel beam expanders and high-power connectors. J Light Technol. 2004;22(1):16–23.
15. Yablon AD. Optical and mechanical effects of frozen-in stresses and strains in optical fibers. IEEE J Sel Top Quantum Electron. 2004;10(2):300–11. https://doi.org/10.1109/JSTQE.2004.826570
16. Durr F, Limberger HG, Salathe RP, Yablon AD. Inelastic strain birefringence in optical fibers. In: OFCNFOEC 2006. 2006 Opt. Fiber Commun. Conf. Natl. Fiber Opt. Eng. Conf. IEEE; 2006. https://doi.org/10.1109/OFC.2006.215442
17. De Senarmont H. Sur les modifications que la réflexion spéculaire à la surface des corps métalliques imprime à un rayon de lumière polarisée. Ann Chim Phys. 1840;73:337–62.
18. Jessop HT. On the Tardy and Sénarmont methods of measuring fractional relative retardations. Br J Appl Phys. 1953;4(5):138–41. https://doi.org/10.1088/0508-3443/4/5/303

19. Goranson RW, Adams LH. A method for the precise measurement of optical path-difference, especially in stressed glass. J Franklin Inst. 1933;216(4):475–504. https://doi.org/10.1016/S0016-0032(33)90918-7
20. Hausmann BD, Miller PA, Aaldenberg EM, Blanchet TA, Tomozawa M. Modeling birefringence in SiO_2 glass fiber using surface stress relaxation. J Am Ceram Soc. 2020;103(3):1666–76. https://doi.org/10.1111/jace.16900
21. Hausmann BD, Aaldenberg EM, Tomozawa M. Photoelastic confirmation of surface stress relaxation in silica glasses: fiber bending and rod torsion. J Am Ceram Soc. 2021;104(7):3087–96. https://doi.org/10.1111/jace.17690
22. Kim BH, Han SR, Paek U-CC, Han W-TT. Diffusion of OH in optical fiber preform by oxy-hydrogen burner. J Non-Cryst Solids. 2004;349(1–3):248–53. https://doi.org/10.1016/j.jnoncrysol.2004.08.150
23. Bacon JF, Hasapis AA, Wholley JW. Viscosity and density of molten silica and high silica content glasses. Phys Chem Glass. 1960;1(3):90–8.
24. Bowen DW, Taylor RW. Silica viscosity from 2300 to 2600 K. Am Ceram Soc Bull. 1978;57(9):818–9.
25. Schultz PC. Fabrication of optical waveguides by the outside vapor deposition process. Proc IEEE. 1980;68(10):1187–90. https://doi.org/10.1109/PROC.1980.11828
26. Tomozawa M, Lezzi PJ, Hepburn RW, Blanchet TA, Cherniak DJ. Surface stress relaxation and resulting residual stress in glass fibers: a new mechanical strengthening mechanism of glasses. J Non-Cryst Solids. 2012;358(18–19):2650–62. https://doi.org/10.1016/j.jnoncrysol.2012.06.018
27. Lezzi PJ, Xiao QR, Tomozawa M, Blanchet TA, Kurkjian CR. Strength increase of silica glass fibers by surface stress relaxation: a new mechanical strengthening method. J Non-Cryst Solids. 2013;379:95–106. https://doi.org/10.1016/j.jnoncrysol.2013.07.033
28. Koike A, Tomozawa M. Deceleration of surface structural relaxation in chlorine-containing silica glass due to chlorine volatilization. J Non-Cryst Solids. 2007;353(30–31):2938–43. https://doi.org/10.1016/J.JNONCRYSOL.2007.06.053

How to cite this article: Hausmann BD, Hawkins TW, Ballato J, Tomozawa M. Effect of draw temperature and flame polishing on birefringence of silica glass fiber. Int J Appl Glass Sci. 2023;1–7. https://doi.org/10.1111/ijag.16623